Fiber Connectivity Integrated Brain Activation Detection

Burak Yoldemir[1], Bernard Ng[2], Todd S. Woodward[3], and Rafeef Abugharbieh[1]

[1] Biomedical Signal and Image Computing Lab, The University of British Columbia, Canada
[2] Parietal Team, INRIA Saclay, France
[3] Department of Psychiatry, The University of British Columbia, Canada
buraky@ece.ubc.ca

Abstract. Inference of brain activation through the analysis of functional magnetic resonance imaging (fMRI) data is seriously confounded by the high level of noise in the observations. To mitigate the effects of noise, we propose incorporating anatomical connectivity into brain activation detection as motivated by how the functional integration of distinct brain areas is facilitated via neural fiber pathways. In this work, we formulate activation detection as a probabilistic graph-based segmentation problem with fiber networks estimated from diffusion MRI (dMRI) data serving as a prior. Our approach is reinforced with a data-driven scheme for refining the connectivity prior to reflect the fact that not all fibers are necessarily deployed during a given cognitive task as well as to account for false fiber tracts arising from limitations of dMRI tractography. Validating on real clinical data collected from 7 schizophrenia patients and 13 matched healthy controls, we show that incorporating anatomical connectivity significantly increases sensitivity in detecting task activation in controls compared to existing univariate techniques. Further, we illustrate how our model enables the detection of significant group activation differences between controls and patients that are missed with standard methods.

Keywords: activation detection, connectivity, dMRI, fMRI, random walker.

1 Introduction

Functional magnetic resonance imaging (fMRI) has become the primary modality for studying human brain activity. To map brain regions to function, standard analysis models the fMRI observations at each voxel as a linear combination of expected temporal responses using the general linear model (GLM) [1]. This univariate approach does not model the integrative property of the brain, which is known to facilitate brain function [2]. To ameliorate this serious limitation, the use of local neighbourhood information has been proposed to regularize activation detection [3, 4]. Although such methods help suppress false spatially-isolated activations by encouraging spatial continuity, they completely ignore long-range functional interactions. The incorporation of functional connectivity information into task activation detection has also been put forth [5], but the approach taken estimates both activation effects and functional connectivity from the same dataset, hence the information gain might be limited. Other works investigated the use of resting-state (RS) functional connectivity information to

J.C. Gee et al. (Eds.): IPMI 2013, LNCS 7917, pp. 135–146, 2013.

inform task activation detection [6] as motivated by the similarity of RS networks and those engaged during task [7]. Given the typically strong noise in fMRI data, exploring other sources of information to regularize activation detection may be beneficial.

Incorporating anatomical information extracted from diffusion MRI (dMRI) data into the investigation of functional brain dynamics has attracted growing interest since functional synchronization between spatially distinct brain regions is enabled through neural fiber pathways [8, 9]. Most of the early work focused on direct comparisons of structural and functional connectivity information learned separately from dMRI and fMRI data [8, 9]. More recently, merits of multi-modal integration for joint anatomical and functional connectivity inference have been explored [10-12]. Promising results in these studies indicate benefits of multi-modal integration though the scope of this strategy has mostly been limited to connectivity estimation.

In this paper, we propose incorporating anatomical connectivity information into task activation detection. Given that fiber pathways serve as the physical substrate for functional interactions, we hypothesize that intrinsically connected brain areas would likely be in similar state, e.g. co-activate, during task [6]. Thus, informing activation detection with anatomical connectivity should presumably improve the detection sensitivity. For this, we employ the graph-theoretic random walker (RW) formulation [13], which easily permits such an integrated scheme for estimating activation probabilities. Posterior activation probabilities estimated by the RW formulation are guaranteed to be unique and globally-optimal [13], which makes RW an eminent choice. RW has been previously applied to task activation detection with functional connectivity taken as the prior [5]. Here, we investigate the implications of complementing task activation detection analysis with anatomical connectivity information. To infer group activation from posterior activation probabilities, we devise a permutation test with activation probabilities as attributes, which we empirically show to provide stronger control on false positive rate than simply comparing the posterior probability of being activated, not activated, and de-activated. On real data, we demonstrate that incorporating anatomical connectivity increases sensitivity in detecting group activation over using univariate techniques. We further show that our method is able to detect significant group activation differences between schizophrenia patients and healthy controls, which are missed by standard analysis approaches.

2 Method

We propose integrating anatomical connectivity into activation effect estimation to improve inference of activation states of brain regions from noisy observations. We use the RW formulation [13] (Section 2.1) to integrate anatomical connectivity learned through tractography (Section 2.2) with the activation likelihood of regions of interest (ROIs) computed using a mixture model applied to activation statistics maps (Section 2.3). Group activation inference is performed on the resulting posterior activation probabilities using a permutation test (Section 2.4). After estimating a group activation pattern, we iteratively refine the anatomical connectivity prior by removing the links between non-active brain regions and re-estimate the posterior activation probabilities until the detected activation pattern stabilizes (Section 2.5). An overview of our multi-modal task activation detection approach is shown in Fig.1.

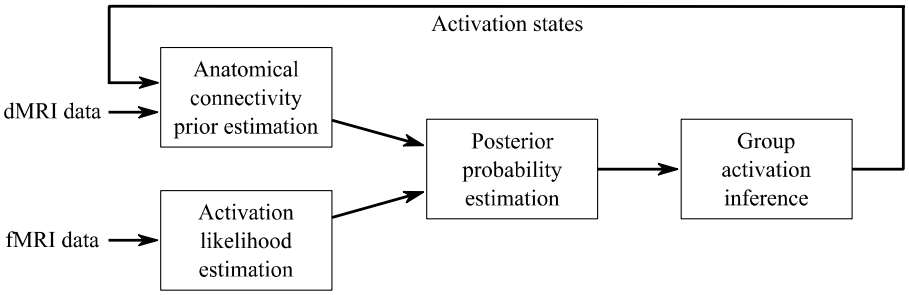

Fig. 1. Overview of proposed multi-modal task activation detection approach. Anatomical connectivity prior and activation likelihood estimates, i.e. label priors, are integrated under the RW formulation to find the posterior activation probabilities. A permutation test is applied on these probabilities to infer group activation. The anatomical connectivity prior is then iteratively refined based on the activation states of the brain regions until convergence.

2.1 Random Walker for Activation Estimation

RW is a graph-based image segmentation approach, in which graph nodes (vertices) correspond to image voxels and graph edges connecting neighbouring nodes are assigned weights reflecting node similarity. In its original formulation [14], RW labels nodes based on the probability that a random walker starting from each node will first reach a pre-labeled seed given edge weights that bias the paths. This requires user-specified seeds and does not utilize local observations at each vertex. Thus, in the context of activation detection with brain regions being the graph nodes and their interactions modeled through graph edges, this would require user-defined seeds for every functionally-disparate region and only functional interactions would be considered without accounting for activation effects. We thus adopt the formulation in [13], which overcomes the need for user interaction and integrates activation effects into the formulation as label priors. This is equivalent to adding a floating vertex for each label and connecting these floating vertices to every vertex in the original graph with label priors being the weights of the added edges [13]. In this formulation, posterior probabilities are calculated by the minimization of the following energy functional:

$$E(\mathbf{x}^s) = \mathbf{x}^{sT}\mathbf{L}\mathbf{x}^s + \sum_{k=1,k\neq s}^{K} \mathbf{x}^{kT}\mathbf{\Lambda}^k\mathbf{x}^k + (\mathbf{x}^s - 1)^T\mathbf{\Lambda}^s(\mathbf{x}^s - 1), \quad (1)$$

where $\mathbf{x}^s$ is an $M\times1$ vector of unknown posterior probabilities of each ROI belonging to class s, $\mathbf{L}$ is an $M\times M$ weighted Laplacian matrix (Section 2.2), $\mathbf{\Lambda}^s$ is an $M\times M$ diagonal matrix having the prior probabilities of the ROIs belonging to class s on its diagonal (Section 2.3), K is the number of class labels, and M is the number of brain regions. The first term in (1) is a spatial term for modeling the interactions between graph vertices as characterized by $\mathbf{L}$. The second term denotes the aspatial component for modeling the local observations at the vertices. In our context of activation detection, the spatial term models the anatomical connectivity information and the aspatial term models the activation effects. The method can thus be thought of as grouping

brain regions into classes via random walk on an augmented graph, where edges in the original graph are weighted by anatomical connectivity information and edges leading to the floating nodes are weighted by activation effects. Assuming equal weighting between the spatial and aspatial energy terms in (1), it has been shown [13] that the posterior probabilities can be found by solving:

$$\left(\mathbf{L}+\sum_{k=1}^{K}\mathbf{\Lambda}^{k}\right)\mathbf{x}^{s}=\boldsymbol{\lambda}^{s}, \tag{2}$$

where $\boldsymbol{\lambda}^{s}$ is an $M\times1$ vector consisting of the diagonal elements of $\mathbf{\Lambda}^{s}$. Since $\mathbf{L}$ is positive semi-definite and $\mathbf{\Lambda}^{k}$ is strictly positive definite, their summation would be diagonally dominant. Hence, matrix inversion is possible for solving (2). Following [15], we set K=3 and define the class labels as deactive, nonactive, and active. For clarity, we explicitly denote the posterior probabilities for each class as $\mathbf{p}_D$, $\mathbf{p}_N$ and $\mathbf{p}_A$, corresponding to deactive, nonactive and active classes, respectively.

2.2 Anatomical Connectivity Prior Estimation

Let $\mathbf{D}$ be an $M\times M$ weighted adjacency matrix**,** where each element $\mathbf{D}_{ij}$ is an estimate of the anatomical connectivity between brain regions i and j, set to fiber count in this work. The corresponding $M\times M$ normalized Laplacian matrix, $\mathbf{L}$, of $\mathbf{D}$ is given by:

$$\mathbf{L}_{ij}=\begin{cases}1 & \text{if } i=j \text{ and } d_j\neq 0\\ -\dfrac{1}{\sqrt{d_i d_j}} & \text{if } i \text{ and } j \text{ are adjacent,}\\ 0 & \text{otherwise}\end{cases} \tag{3}$$

where $d_i=\Sigma_j\,\mathbf{D}_{ij}$ is the degree of node i. A major difficulty with tractography is resolving fiber crossing regions where accuracy of most algorithms is seriously affected. In [16], it was proposed that multiplying $\mathbf{D}$ by itself may help address this problem by generating multi-step fibers from parts of fibers that might be split at crossing regions:

$$\mathbf{D}^{MS}=\exp(\mathbf{D})=\sum_{k=0}^{\infty}\frac{1}{k!}\mathbf{D}^{k}, \tag{4}$$

where exp(·) denotes the matrix exponential. $\mathbf{D}^{k}$=**D*****D*****D***... and $\mathbf{D}^{k}_{ij}$ is the number of paths of length k connecting regions i and j. $\mathbf{D}^{MS}$ hence comprises all possible paths between each region pair, where indirect paths are more heavily penalized as these paths are potentially artifactual [16].

2.3 Activation Likelihood Estimation

To estimate the activation likelihoods, which are used as label priors $\boldsymbol{\lambda}^{s}$ in RW, we first apply the classical GLM [1] to compute the intra-subject activation statistics:

$$\begin{aligned} \mathbf{y}_j &= \mathbf{X}\boldsymbol{\beta}_j + \mathbf{e}_j \\ \mathbf{t}_j &= \hat{\boldsymbol{\beta}}_j / se(\hat{\boldsymbol{\beta}}_j), \end{aligned} \tag{5}$$

where $\mathbf{y}_j$ is the $n\times1$ time course of ROI j, $\mathbf{X}$ is the $n\times r$ design matrix of expected responses, $\hat{\boldsymbol{\beta}}_j$ is an $r\times1$ vector containing estimates of the activation effects, $\boldsymbol{\beta}_j$, $\mathbf{e}_j$ is the $n\times1$ residual assumed to be white Gaussian noise after preprocessing, $se(\hat{\boldsymbol{\beta}}_j)$ is the standard error of $\hat{\boldsymbol{\beta}}_j$, $\mathbf{t}_j$ is the $r\times1$ vector of sought activation statistics, n is the number of time points, and r is the number of experimental conditions. Columns of the design matrix $\mathbf{X}$ are generated by convolving the canonical hemodynamic response function (HRF) with a boxcar time-locked to stimulus [1]. To compute the prior probabilities of ROIs belonging to each class, we fit a Gamma-Gaussian-Gamma (GGG) mixture model separately to the t-values of each condition, $\mathbf{t}^c$, i.e. c^{th} element of $\mathbf{t}_j$ assembled across all ROIs [15]. The Gaussian distribution models the nonactive state and the Gamma distributions model the deactive and active states:

$$\mathbf{t}_j^c \sim \pi_D \Gamma(k_D, \theta_D) + \pi_N N(\mu, \sigma) + \pi_A \Gamma(k_A, \theta_A), \tag{6}$$

where μ is the mean and σ is the standard deviation of the Gaussian component, k_D and k_A are the shape parameters, and θ_D and θ_A are the scale parameters of the deactivation (D) and activation (A) components, respectively. We employ the expectation-maximization (EM) algorithm [17] to estimate the model parameters separately for each experimental condition c with the probabilities of $\mathbf{t}^c$ given the parameter estimates used as the label priors $\boldsymbol{\lambda}^s$. These label priors and the Laplacian matrix given in Section 2.2 are combined through (2) to estimate the posterior activation probabilities.

2.4 Group Activation Inference

The high dimensionality of fMRI data elicits a high risk of false detection. To infer group activation from activation statistics, such as t-values, several methods that control for false positive rate have been proposed, e.g. Bonferroni correction, Gaussian random field theory, max-t permutation test [18]. For group activation inference from posterior activation probability maps, most studies directly threshold the posterior activation probabilities at $1/K$, where K is the number of classes, arguing that activation inference from posterior activation probabilities does not suffer from false positives [19]. However, as we will empirically demonstrate in Section 4, directly thresholding the posterior probabilities is actually prone to false detection, necessitating a more rigorous activation inference method. To this end, we propose a permutation test for group inference from activation probabilities that controls for the false positive rate. Specifically, for each permutation, we first randomly select one third of the subjects and swap the posterior probabilities $\mathbf{p}_A$ and $\mathbf{p}_D$ of each selected subject. We note that this swap is done at the intra-subject level for all ROIs, hence the spatial pattern of the activation probabilities is preserved. Similarly, we swap $\mathbf{p}_A$ and $\mathbf{p}_N$ for another third of randomly selected subjects. We then compute the z-scores of $\mathbf{p}_A$ for each permutation across all subjects. This procedure is repeated 10,000 times to generate the null distribution of activation probabilities of each ROI. We assign the p-value for

the activation likelihood of each ROI as the number of times the z-scores of permuted $\mathbf{p}_A$ are greater than the z-scores of the original $\mathbf{p}_A$ values divided by the total number of trials (in this case, 10,000). Under the null hypothesis that there is no activation, the z-score of the original $\mathbf{p}_A$ value of an ROI would lie around the mean of the generated null distribution, resulting in a non-significant p-value around 0.5. Finally, false discovery rate (FDR) [20] is applied to these p-values to account for multiple comparisons. As shown in Section 4 on a synthetic case, this permutation test offers a much lower false positive rate compared to posterior probability thresholding while keeping the true positive rate at the same (or even at a higher) rate.

2.5 Re-estimation of Group Activation Using Partial Connectome

Since some of the estimated fiber tracts might be false due to tractography errors and not all fibers are necessarily employed during a given cognitive task, we propose restricting the anatomical connectivity prior to the subset of fibers that are likely to be active by iteratively refining the original connectivity prior, $\mathbf{D}^{orig}$, as follows:

$$\mathbf{D}^{m+1} = \mathbf{D}^{task} + \frac{1}{\log(m+1)}\mathbf{D}^{m}, \tag{7}$$

$$\mathbf{D}_{ij}^{task} = \begin{cases} \mathbf{D}_{ij}^{orig} & \text{if } l_i^m \vee l_j^m = 1 \\ 0 & \text{if } l_i^m = l_j^m = 0 \end{cases}, \tag{8}$$

where $\mathbf{D}^m$ is the $M \times M$ partial adjacency matrix found in iteration m with $\mathbf{D}^1$ set to $\mathbf{D}^{orig}$. l_i^m is the estimated activation state of ROI i during iteration m with a value of 1 denoting activated and 0 denoting not activated or deactivated. We note that updating $\mathbf{D}^{orig}$ using the above scheme enables $\mathbf{D}^{orig}$ to gradually evolve as opposed to having its information from previous iterations completely discarded. The overall process proceeds by estimating the group activation map with $\mathbf{D}^1$ as the prior. We then refine $\mathbf{D}^1$ using (7) and (8), and repeat the process until the group activation map stabilizes.

3 Materials

After obtaining informed consent, fMRI data were collected from 13 healthy subjects (6 men, 7 women, mean age 27.46±6.38 years) and 7 schizophrenia patients (5 men, 2 women, mean age 30.57±10.08 years). Each subject was first presented with words in four different contexts: associating, hearing, solving and reading, during a non-scanned encoding session. The subjects were then presented the same set of words in a subsequent recall run during which fMRI data were acquired and subjects were asked to indicate the context in which the presented words were previously encountered. Image acquisition was performed on a Philips Achieva 3.0 T MRI scanner using a T2*-weighted gradient-echo spin pulse sequence with a repetition time of 2000 ms, an echo time of 30 ms, a flip angle of 90°, a field of view of 240×240 mm, and an in-plane resolution of 80×80 pixels. Each volume comprised 36 axial slices of 3 mm thickness with a 1 mm gap. Each scan lasted for 920 s, which tallies to 460 fMRI

volumes. For each subject's data, motion correction and spatial normalization were performed using SPM8. The voxel time courses were then high-pass filtered to remove drifts and temporally whitened using an AR(1) model. For computing fiber count, we parcellated the brain into 500 ROIs [21] by applying Ward clustering [22] on voxel time courses concatenated across subjects. Voxel time courses within each ROI were averaged to generate ROI time courses.

dMRI data were collected from the same subjects using a Philips Achieva 3.0 T MRI scanner with a TR of 7500 ms, a TE of 54 ms, an EPI factor of 59, an FOV of 224×224 mm and an in-plane resolution of 256×256 pixels. Fifteen diffusion weighted volumes were acquired at a b-value of 800 s/mm^2 in addition to a volume with no diffusion sensitization. Each volume consisted of 72 slices of 2 mm thickness with no gap. Acquisition time was 480 s. We used FSL [23] for eddy current correction and MedINRIA [24] for diffusion tensor estimation and fiber tractography. To facilitate the computation of fiber count, we warped our functionally derived group parcel map to the B0 volume of each subject.

4 Results and Discussion

We first present the synthetic test performed to assess our proposed permutation test (Section 2.4) as compared to the posterior probability thresholding approach commonly employed in the literature [19]. For evaluation on real data, we compare the sensitivity of our proposed approach in detecting group activation in controls against that of univariate techniques. We then contrast our method against classical schemes in detecting group activation differences between schizophrenia patients and controls.

Synthetic Test of Group Inference Strategies. We performed a synthetic test carefully designed from activation probabilities calculated from the real data of healthy controls. Specifically, after estimating the group activation map with our approach, we used the highest one third of $\mathbf{p}_N$ among nonactive ROIs and the highest one third of $\mathbf{p}_A$ among active ROIs to generate a pseudo ground truth of nonactivation and activation probability distributions at the intra-subject level. These pseudo ground truth distributions are assumed to be Gaussian with means and standard deviations set to that of the respective thirds of $\mathbf{p}_N$ and $\mathbf{p}_A$. Out of a total of 100 synthetic datasets, each dataset comprised 13 subjects having 500 ROIs each, with 100 of them defined to be active. Random samples of $\mathbf{p}_N$ and $\mathbf{p}_A$ were drawn for each subject from the corresponding probability distributions. Deactivation probabilities were computed based on how posterior probabilities should sum to 1. Assessing group activation with the proposed permutation test resulted in a true positive rate (TP) of 0.819±0.038 and a false positive rate (FP) of 0.008±0.004, whereas thresholding $\mathbf{p}_A$ at 1/3 gave a TP of 0.374±0.049 and an FP of 0.097±0.015. One-sample t-tests among TPs and FPs of these two strategies declared the differences to be significant at $p<10^{-6}$, demonstrating superior sensitivity and specificity.

Detecting Group Activation in Controls. We compare the sensitivity of our method against classical GLM and against inferring group activation from the activation likelihoods given by the GGG mixture model. We further compare the effect of using $\mathbf{D}$ and $\mathbf{D}^{MS}$ as the anatomical connectivity estimates (Section 2.2). Fig. 2 shows the

number of detected ROIs for different p-value thresholds. Our approach is denoted as RW for the first iteration where the full anatomical adjacency matrix is used, and RW_{it} for the following iterations with partial adjacency matrices. For the same specificity, our approach provided higher detection sensitivity than using the activation likelihoods given by the GGG mixture model, implicating the advantage of incorporating anatomical connectivity into activation detection. Iterating the procedure with refined anatomical connectivity estimates considerably improved detection. The procedure was iterated 100 times and for clarity, only the mean and standard deviations for the iterations with partial adjacency matrices were provided. It was observed that group activation map stabilized after 100 iterations, with only a couple of parcels changing labels in further iterations. This additional improvement provided by the refinement of the anatomical connectivity estimate suggests that only a subset of fibers is employed during a given task. Hence, isolating the utilized fibers can be beneficial. The improvement could also be partly due to removal of false fiber tracts arising from tractography errors. GLM (FDR corrected) provides more detection than our method at more liberal thresholds, but its performance varies considerably with p-value thresholds. In contrast, our method provides more consistent results across p-values. Comparing the results of using the original anatomical adjacency matrix versus the multi-step counterpart (denoted as RW-MS for the first, $RW\text{-}MS_{it}$ for the following iterations) suggests that some of the artifactual connections generated by the multi-step approach likely do not pertain to task activation.

Qualitatively, the ROIs detected across all experimental conditions in healthy controls largely match regions known to be involved in context memory tasks [25], which further validates our method. As shown in Fig. 3, the areas detected across all conditions include superior frontal gyrus, middle frontal gyrus, inferior frontal gyrus, supramarginal gyrus, precentral gyrus, postcentral gyrus, angular gyrus, lateral occipital cortex, occipital pole, cingulate gyrus, lingual gyrus, hippocampus and insula.

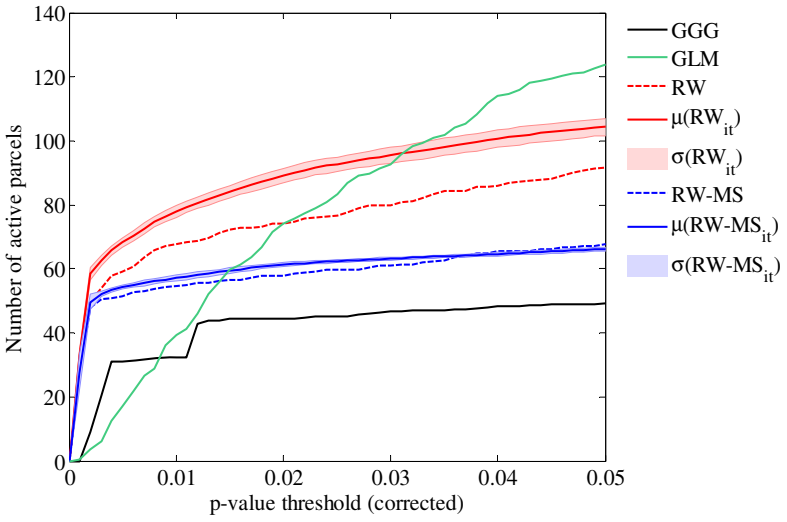

Fig. 2. Quantitative activation detection comparison

Detecting Differences between Patients and Controls. To assess the significant activation differences between schizophrenia patients and control subjects, we compared two different types of context memory recall: (1) self-other source information monitoring (did I say this word or did I hear it?) and (2) task information monitoring (did I produce a semantic associate of this word or did I read it?). Both types of context memory are thought to be impaired in schizophrenia. This comparison corresponds to the contrast between associating/reading and solving/hearing conditions. We employed a max-t permutation test [18] on the $\mathbf{p}_A$ values of the two groups

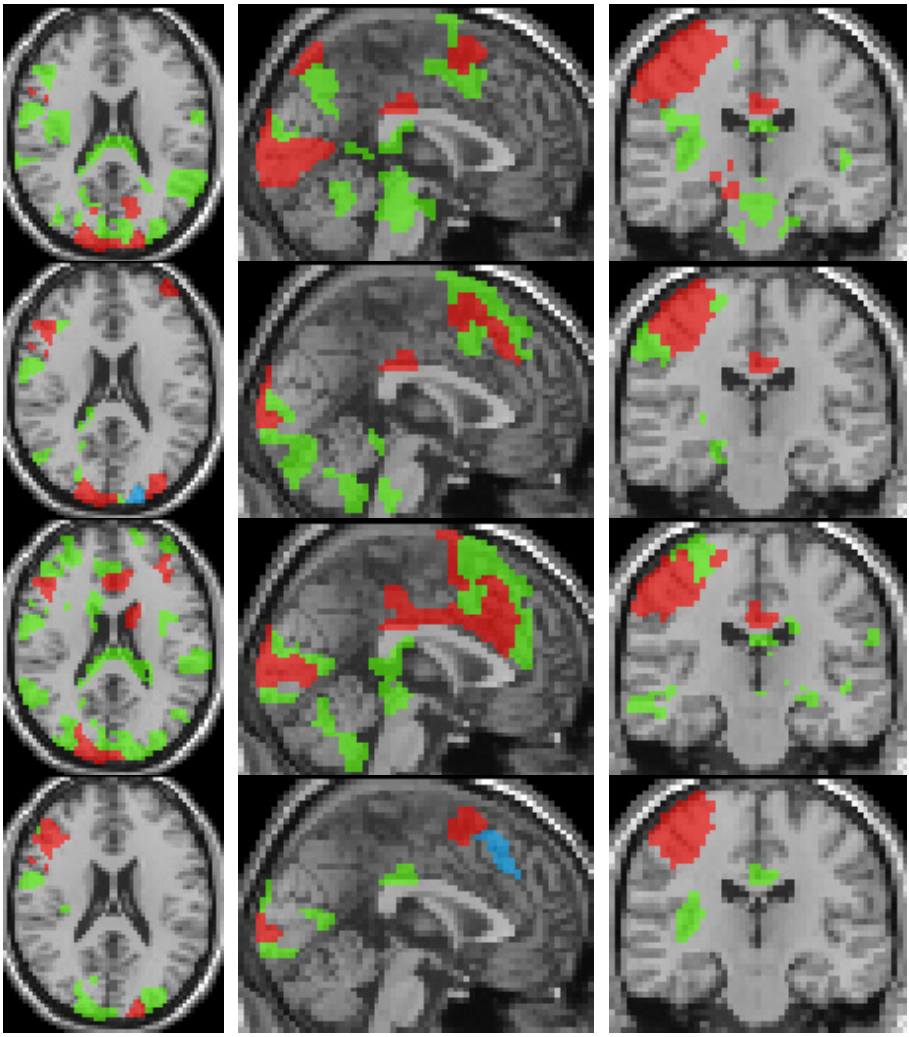

Fig. 3. Activation patterns detected at p-value < 0.05. Green=detected by RW only. Blue=detected by GGG only. Red=detected both by RW and GGG. Each row corresponds to an experimental condition, top-to-bottom: associating, hearing, solving, reading.

for this contrast and observed a significant difference ($p<0.05$, corrected) in the left hippocampus. Activity in this region was higher in the source monitoring condition for schizophrenia patients relative to controls but lower in the task monitoring condition relative to controls. Applying the same test on the results of GLM or GGG mixture modeling approach failed to detect any group differences up to $p<0.2$. The left hippocampus is involved in reactivation and association of stored semantic knowledge to consolidate new information into existing semantic frameworks [26-28]. The implication of the significant difference in the left hippocampus is that, aberrant activity in this region could lead to different manifestations of poor performance in context memory. Reduced activity during task monitoring could relate to the episodic memory impairments commonly observed in schizophrenia [29], which implies that underactivity in this region would lead to reduced reactivation of stored semantic knowledge for context memory. Increased activity during source monitoring could relate to the source memory impairments commonly observed in schizophrenia [30], such that overactivity in this region would lead to increased perceptual context for both self and other source information, leading to more difficulty in distinguishing between these two sources in context memory.

5 Conclusions

We proposed a novel fiber connectivity integrated approach for group activation inference. On real data of healthy subjects, we demonstrated that integrating dMRI and fMRI significantly increases sensitivity in detecting group activation compared to analyzing fMRI data alone. We further showed that incorporating a refined connectome comprising anatomical connections linked only to the estimated active brain regions results in improved performance over using the full estimated connectome. Finally, we presented novel findings in activation differences between healthy controls and schizophrenia patients that were missed with standard methods. Our multimodal integration strategy thus holds great promise for brain activity analysis.

Acknowledgements. This work is partly funded by NSERC and the Institute for Computing, Information and Cognitive Systems (ICICS) at UBC.

References

1. Friston, K.J., Holmes, A.P., Worsley, K.J., Poline, J.B., Frith, C.D., Frackowiak, R.S.J.: Statistical Parametric Maps in Functional Imaging: A General Linear Approach. Hum. Brain Mapp. 2, 189–210 (1995)
2. Rogers, B.P., Morgan, V.L., Newton, A.T., Gore, J.C.: Assessing Functional Connectivity in the Human Brain by fMRI. Magn. Reson. Imaging 25, 1347–1357 (2007)
3. Descombes, X., Kruggel, F., von Cramon, D.Y.: Spatio-Temporal fMRI Analysis Using Markov Random Fields. IEEE Trans. Med. Imaging 17, 1028–1039 (1998)
4. Penny, W.D., Trujillo-Barreto, N.J., Friston, K.J.: Bayesian fMRI Time Series Analysis with Spatial Priors. NeuroImage 24, 350–362 (2005)

5. Ng, B., Abugharbieh, R., Hamarneh, G., McKeown, M.J.: Random Walker Based Estimation and Spatial Analysis of Probabilistic fMRI Activation Maps. In: MICCAI fMRI Data Analysis Workshop, pp. 37–44 (2009)
6. Ng, B., Abugharbieh, R., Varoquaux, G., Poline, J.B., Thirion, B.: Connectivity-Informed fMRI Activation Detection. In: Fichtinger, G., Martel, A., Peters, T. (eds.) MICCAI 2011, Part II. LNCS, vol. 6892, pp. 285–292. Springer, Heidelberg (2011)
7. Smith, S.M., Fox, P.T., Miller, K.L., Glahn, D.C., Fox, P.M., Mackay, C.E., Filippini, N., Watkins, K.E., Toro, R., Laird, A.R., Beckmann, C.F.: Correspondence of the Brain's Functional Architecture During Activation and Rest. Proc. Natl. Acad. Sci. 106, 13040–13045 (2009)
8. Honey, C.J., Thivierge, J.P., Sporns, O.: Can Structure Predict Function in the Human Brain? NeuroImage 52, 766–776 (2010)
9. Damoiseaux, J.S., Greicius, M.D.: Greater than the Sum of its Parts: A Review of Studies Combining Structural Connectivity and Resting-State Functional Connectivity. Brain Struct. Funct. 213, 525–533 (2009)
10. Ng, B., Varoquaux, G., Poline, J.-B., Thirion, B.: A Novel Sparse Graphical Approach for Multimodal Brain Connectivity Inference. In: Ayache, N., Delingette, H., Golland, P., Mori, K. (eds.) MICCAI 2012, Part I. LNCS, vol. 7510, pp. 707–714. Springer, Heidelberg (2012)
11. Venkataraman, A., Rathi, Y., Kubicki, M., Westin, C.F., Golland, P.: Joint Modeling of Anatomical and Functional Connectivity for Population Studies. IEEE Trans. Med. Imaging 31, 164–182 (2012)
12. Chen, H., Li, K., Zhu, D., Zhang, T., Jin, C., Guo, L., Li, L., Liu, T.: Inferring Group-Wise Consistent Multimodal Brain Networks via Multi-view Spectral Clustering. In: Ayache, N., Delingette, H., Golland, P., Mori, K. (eds.) MICCAI 2012, Part III. LNCS, vol. 7512, pp. 297–304. Springer, Heidelberg (2012)
13. Grady, L.: Multilabel Random Walker Image Segmentation Using Prior Models. In: Proc. IEEE Comp. Soc. Conf. Comp. Vision Pattern Recog., vol. 1, pp. 763–770 (2005)
14. Grady, L.: Random Walks for Image Segmentation. IEEE Trans. Pattern Anal. Mach. Intell. 28, 1768–1783 (2006)
15. Hartvig, N.V., Jensen, J.L.: Spatial Mixture Modeling of fMRI Data. Hum. Brain Mapp. 11, 233–248 (2000)
16. Skudlarski, P., Jagannathan, K., Calhoun, V.D., Hampson, M., Skudlarska, B.A., Pearlson, G.: Measuring Brain Connectivity: Diffusion Tensor Imaging Validates Resting State Temporal Correlations. NeuroImage 43, 554–561 (2008)
17. Dempster, A.P., Laird, N.M., Rubin, D.B.: Maximum Likelihood from Incomplete Data via the EM Algorithm. J. R. Statist. Soc. B 39, 1–38 (1977)
18. Nichols, T., Hayasaka, S.: Controlling the Familywise Error Rate in Functional Neuroimaging: A Comparative Review. Stat. Methods Med. Research 12, 419–446 (2003)
19. Friston, K.J., Penny, W.: Posterior Probability Maps and SPMs. NeuroImage 19, 1240–1249 (2003)
20. Genovese, C.R., Lazar, N.A., Nichols, T.: Thresholding of Statistical Maps in Functional Neuroimaging Using the False Discovery Rate. NeuroImage 15, 870–878 (2002)
21. Thyreau, B., Thirion, B., Flandin, G., Poline, J.-B.: Anatomo-Functional Description of the Brain: A Probabilistic Approach. In: IEEE Int. Conf. Acoustics, Speech and Signal Proc., vol. 5, pp. 14–19 (2006)
22. Michel, V., Gramfort, A., Varoquaux, G., Eger, E., Keribin, C., Thirion, B.: A Supervised Clustering Approach for fMRI-based Inference of Brain States. Patt. Recog. 45, 2041–2049 (2012)

23. Smith, S.M., Jenkinson, M., Woolrich, M.W., Beckmann, C.F., Behrens, T.E.J., Johansen-Berg, H., Bannister, P.R., De Luca, M., Drobnjak, I., Flitney, D.E., Niazy, R., Saunders, J., Vickers, J., Zhang, Y., De Stefano, N., Brady, J.M., Matthews, P.M.: Advances in Functional and Structural MR Image Analysis and Implementation as FSL. NeuroImage 23, 208–219 (2004)
24. Toussaint, N., Souplet, J.C., Fillard, P.: MedINRIA: Medical Image Navigation and Research Tool by INRIA. In: MICCAI Workshop on Interaction in Medical Image Analysis and Visualization, pp. 1–8 (2007)
25. Wang, L., Metzak, P.D., Honer, W.G., Woodward, T.S.: Impaired Efficiency of Functional Networks Underlying Episodic Memory-for-Context in Schizophrenia. J. Neurosci. 30, 13171–13179 (2010)
26. Eichenbaum, H.: Conscious Awareness, Memory and the Hippocampus. Nat. Neurosci. 2, 775–776 (1999)
27. Henke, K., Weber, B., Kneifel, S., Wieser, H.G., Buck, A.: Human Hippocampus Associates Information in Memory. Proc. Natl. Acad. Sci. 96, 5884–5889 (1999)
28. Giovanello, K.S., Schnyer, D.M., Verfaellie, M.: A Critical Role for the Anterior Hippocampus in Relational Memory: Evidence from an fMRI Study Comparing Associative and Item Recognition. Hippocampus 14, 5–8 (2004)
29. Heinrichs, W., Zakzanis, K.K.: Neurocognitive Deficit in Schizophrenia: A Quantitative Review of the Evidence. Neuropsychology 12, 426–445 (1998)
30. Waters, F., Woodward, T.S., Allen, P., Aleman, A., Sommer, I.: Self-recognition Deficits in Schizophrenia Patients with Auditory Hallucinations: A Meta-analysis of the Literature. Schizophrenia Bulletin 38, 741–750 (2012)